

Supporting information

Grafting Rh-bipyridine complex on carbon nitride through coordination: ligand modification of single-atomic Rh for enhanced CO₂ reduction and inhibited H⁺ reduction

Ling Li^a, Yulu Mao^a, Jiwu Zhao^b, Yuxuan Zhang^a, Han Wu^a, Quan Gu^{a,}*

^a Key Laboratory of Applied Surface and Colloid Chemistry, Ministry of Education, Xi'an Key Laboratory of Organometallic Material Chemistry, School of Chemistry and Chemical Engineering, Shaanxi Normal University, Xi'an, 710062, P. R. China.

^b State Key Laboratory of Photocatalysis on Energy and Environment, College of Chemistry, Fuzhou University, Fuzhou, 350116, China

*E-mail: guquan@snnu.edu.cn

1. Experimental section

1.1. Chemicals and reagents

Melamine (99%), urea (AR), and sodium borohydride (98%) were purchased from Aladdin. Anhydrous lithium chloride (AR), sodium chloride (AR), and potassium chloride (AR) were obtained from Guangzhou Jinhuada Chemical Reagent Co., Ltd. Rhodium chloride hydrate (AR, 99.9%) was obtained from Alfa Aesar. Triethanolamine (TEOA, AR) and acetonitrile (AR), were purchased from Sinopharm Chemical Reagent Co., Ltd. Chloroplatinic acid hydrate ($\text{H}_2\text{PtCl}_6 \cdot x\text{H}_2\text{O}$, 99.95%) was obtained from Innochem. 2,2'-bipyridine (98%), 4,4'-dimethyl-2,2'-dipyridyl (98%), 4,4'-di-tert-butyl-2,2'-dipyridyl (98%), 4,4'-dibromo-2,2'-bipyridyl (98%), 2,2'-bipyridine-4,4'-dicarboxylic acid (96%), 5,5'-dimethyl-2,2'-bipyridyl (98%), 2,2':6',2''-terpyridine (98%), 4'-chloro-2,2':6',2''-terpyridine (98%) were purchased from Energy Chemical. All the chemicals are unpurified before use.

1.2. Preparation of CN-bpy

20 mg of CN and 15 mg of 2,2'-bipyridine were added to a mixed solution of 3 mL of acetonitrile (CH_3CN), 1.0 mL of triethanolamine (TEOA), and 1.0 mL of deionized water in the reactor. After that, the suspension was degassed with carbon dioxide for 20 min under vigorous stirring to remove the air in the system before light irradiation. After reacting under light for a period (10h), the precipitate (CN-bpy) was collected via centrifugation, and washed with deionized water three times, dried at 60 °C in a vacuum oven.

1.3. Preparation of carbon nitride nanosheets (CNNS)

Urea (30 g) was fully ground in an agate mortar for 30 min and the mixture was placed in a crucible and annealed at 550 °C for 4 h with a heating rate of 2.5 °C min^{-1} under an air atmosphere in a muffle furnace. The obtained powder was then annealed at 500 °C for 4 h with a heating rate of 5 °C min^{-1} under an air atmosphere in a muffle furnace to obtain carbon nitride nanosheets (CNNS).

1.4. Preparation of Rh_1/CNNS and $\text{Rh}_1\text{-bpy}/\text{CNNS}$

100 mg CNNS were dispersed in 30 mL deionized water to obtain the suspension under vigorous stirring in a round-bottomed flask. 0.3 mL of RhCl_3 solution (2.5 mg Rh/mL) was added into 4 mL NaCl solution (20 mg NaCl). Then, a certain amount of the above aqueous solution was added into 30 mL CNNS suspension under vigorous

stirring. The resulting mixture was heated at 80 °C for 8 h. After that, the resulting product was collected by centrifugation, and washed with deionized water several times, followed by drying in a vacuum oven. The obtained powder was dispersed in 15 mL of deionized water in a beaker under stirring and the suspension was irradiated by a 300 W Xe lamp for 1 h in Ar atmosphere at room temperature. Finally, the product was collected via centrifugation, and washed with deionized water three times, dried at 60 °C in a vacuum oven.

20 mg of Rh₁/CNNS and 15 mg of 2,2'-bipyridine (bpy) were added to a mixed solution of 3 mL of acetonitrile (CH₃CN), 1.0 mL of triethanolamine (TEOA), and 1.0 mL of deionized water in the reactor. After that, the suspension was degassed with carbon dioxide for 20 min under vigorous stirring to remove the air in the system before light irradiation. After reacting under light for a period, the precipitate (Rh₁-bpy/CNNS) was collected via centrifugation, and washed with deionized water three times, dried at 60 °C in a vacuum oven.

1.5. Preparation of CNNS/RhCl₃ and CNNS/RhCl₃-bpy

The resulting sample recovered after the one-pot photocatalytic reaction (CNNS-RhCl₃-2,2'-bipyridine system) was denoted as CNNS/RhCl₃-bpy. Typically, 20 mg of CNNS and 15 mg of 2,2'-bipyridine were added to a mixed solution of 3 mL of acetonitrile (CH₃CN), 1.0 mL of triethanolamine (TEOA), and 1.0 mL of deionized water in the reactor. Then, a certain amount of RhCl₃ solution (2.5 mg Rh/mL) was added into CN suspension under vigorous stirring. After that, the suspension was degassed with carbon dioxide for 20 min under vigorous stirring to remove the air in the system before light irradiation. After reacting under light for a period, the precipitate (CNNS/RhCl₃-bpy) was collected via centrifugation, and washed with deionized water three times, dried at 60 °C in a vacuum oven. The sample obtained by using the same method without adding 2,2'-bipyridine is labeled as CNNS/RhCl₃.

1.6. Preparation of Rh NPs/CN and Pt NPs/CN

100 mg CN powder was dispersed in 30 mL methanol under vigorous stirring in a beaker. Then, a certain amount of RhCl₃ solution (2.5 mg Rh/mL) or H₂PtCl₆ solution (6.59 mg Pt/mL) was added into the above suspension under vigorous stirring for 0.5 h. Then, 20 mL NaBH₄ was added into the above suspension and the suspension was kept stirring for 10 h. After that, the sample was collected by centrifugation, washed with deionized water, ethanol, and acetone several times, followed by drying at 80 °C.

1.7. Preparation of Pt₁/CN

0.3 mL of H_2PtCl_6 solution (6.59 mg Pt/mL) was added into 4 mL NaCl solution (20 mg NaCl). Then, a certain amount of the above aqueous solution was added into 30 mL CN suspension (100 mg CN were dispersed in 30 mL deionized water) under vigorous stirring in a beaker. The resulting mixture was heated at 80 °C for 8 h. After that, the resulting product was collected by centrifugation, and washed with deionized water several times, followed by drying in a vacuum oven. The obtained powder was dispersed in 15 mL of deionized water in a beaker under stirring and the suspension was irradiated by a 300 W Xe lamp for 1 h in an Ar atmosphere at room temperature. Finally, the product was collected via centrifugation, and washed with deionized water three times, by drying at 60 °C in a vacuum oven.

1.8. Characterization

The X-ray diffraction (XRD) measurements of all samples were performed on a Bruker D8 Advance X-ray diffractometer using $\text{CuK}\alpha 1$ radiation ($\lambda = 1.5418 \text{ \AA}$). The accelerating voltage and the applied current were 40 kV and 40 mA, respectively. The XRD patterns were collected from $2\theta=5$ to 80° at a scan rate of $2.4^\circ \text{ min}^{-1}$.

Scanning electron microscopy (SEM) images were obtained on a field emission scanning electron microscope (HITACHI SU8220 microscope) at an acceleration voltage and the applied current of 5 kV and 10 μA . For the SEM test, the powder samples were glued on an aluminum SEM specimen holder with the conductive resin, and then the specimen holder was directly put into SEM for testing without gold spraying.

Transmission electron microscopy (TEM) images and element mapping were obtained by a Tecnai G2 F20 transmission electron microscopy (FEI, USA) at an accelerating voltage of 200 kV. A small amount of the sample was dispersed in 1 mL ethanol and the mixture was then sonicated for 30 min at room temperature in a bath sonicator. The obtained suspension was dropped on 230-mesh carbon-coated copper grids and air-dried for TEM measurements.

The aberration-corrected high-angle annular dark-field scanning TEM (HAADF-STEM) and Energy-Dispersive X-ray spectroscopy (EDS) mapping were acquired on JEOL-ARM200F transmission electron microscopy.

X-ray absorption fine structure spectra (XAFS) were acquired at the BL14W beamline of the Shanghai Synchrotron Radiation Facility (SSRF) using the SSRF storage ring at 3.5 GeV with a stabilization current of 200 mA. The data were collected

in fluorescence mode with a Lytle detector using a Si (111) two-crystal monochromator. All spectra were collected in ambient conditions.

X-ray photoelectron spectra (XPS) of the samples were obtained on a VG ESCALAB 250 XPS system with a monochromatized Al K α X-ray source (15 kV, 200 W).

UV-vis diffuse reflectance spectra (UV-vis DRS) were measured by a UV/vis spectrophotometer (UV-Lambda 950, Perkin Elmer).

Fourier Transform Infrared (FTIR) spectra were derived from Perkin Elmer Fourier transform infrared spectrometer GX.

For photoelectrochemical experiments, the as-prepared sample was coated on fluorine-doped tin oxide (FTO) glass as the working electrode. Typically, the FTO glass with a size of 1.0 \times 2.0 cm was washed in turn with acetone, ethanol, and DI water under continuous sonication, and then dried in N₂ flowing. By dispersing a certain amount of the sample in water, the sample slurry was obtained and used for spreading onto the cleaned FTO glass substrate (photoactive area of 0.25 cm²) and dried at room temperature. The photoelectrochemical tests were performed on a CHI 760E electrochemical work station (Chenhua Instrument, Shanghai, China) at room temperature in a standard three-electrode system including a working electrode, a platinum wire counter electrode, and an Ag/AgCl reference electrode. The working electrode was immersed in a sodium sulfate electrolyte solution (0.5 M) and irradiated by visible light. The chopped anodic photocurrent (i-t curve) of samples was tested at an applied bias of 0.6 V vs Ag/AgCl. Electrochemical Impedance Spectroscopy (EIS) measurement was conducted in a frequency range of 0.01 Hz to 10 kHz for an amplitude of 5 mV.

1.9. Density function theory (DFT) calculation methods

The DFT calculations were performed on Vienna Ab-initio Simulation Package (VASP) coded^{1, 2}. The electron-ion interaction was treated by projector augmented wave (PAW) pseudopotential^{3, 4} and the exchange-correlation function was described by generalized gradient approximation with Perdew-Burke-Ernzerhof (GGA-PBE) method⁵. During the geometry optimization of the models, a 15 Ångström-thick vacuum layer was used to eliminate the interaction between two adjacent slabs. The kinetic energy cutoff of 500 eV was used to control the optimization convergence. This study considered that geometry optimization is convergence until the convergence criteria of energy and force reached 1 \times 10⁻⁶ eV and 0.02 eV Å⁻¹, respectively. The Brillouin zone was sampled on the Gamma-centered Monkhorst-Pack (MP) grids⁶, and

the k-point was set to 1×1×3 for all the models. The DFT-D3(BJ) method^{7, 8} was used to account for the vdW-dispersion energy-correction. The data processing was assisted by VASPKIT⁹, QVASP¹⁰, and VESTA¹¹ software. The Gibbs free energy difference (ΔG) is defined as:¹²

$$\Delta G = \Delta E + \Delta ZPE - T\Delta S$$

Where E, ZPE, T, and S represent the energy from DFT calculation, zero-point energy, temperature (298.15 K), and entropy, respectively.

1. G. Kresse, J. Furthmüller, *Comput. Phys. Commun.* **6**, 15-50 (1996).
2. G. Kresse, J. Furthmüller, *Phys. Rev. B* **54**, 11169-11186 (1996).
3. G. Kresse, D. Joubert, *Phys. Rev. B* **59**, 1758-1775 (1999).
4. P. E. Blöchl, *Phys. Rev. B* **50**, 17953-17979 (1994).
5. J. P. Perdew, K. Burke, M. Ernzerhof, *Phys. Rev. Lett.* **77**, 3865-3868 (1996).
6. S. Froyen, *Phys. Rev. B* **39**, 3168-3172 (1989).
7. S. Grimme, J. Antony, S. Ehrlich, H. Krieg, *J. Chem. Phys.* **132**, 154104 (2010).
8. S. Grimme, S. Ehrlich, L. Goerigk, *J. Comput. Chem.* **32**, 1456-1465 (2011).
9. V. Wang, N. Xu, J.-C. Liu, G. Tang, W.-T. Geng, *Comput. Phys. Commun.* **267**, 108033 (2021).
10. W. Yi, G. Tang, X. Chen, B. Yang, X. Liu, *Comput. Phys. Commun.* **257**, 107535 (2020).
11. K. Momma, F. Izumi, *J. Appl. Crystallogr.* **44**, 1272-1276 (2011).
12. J. K. Nørskov *et al.*, *J. Phys. Chem. B* **108**, 17886-17892 (2004).

2. Figures and Tables

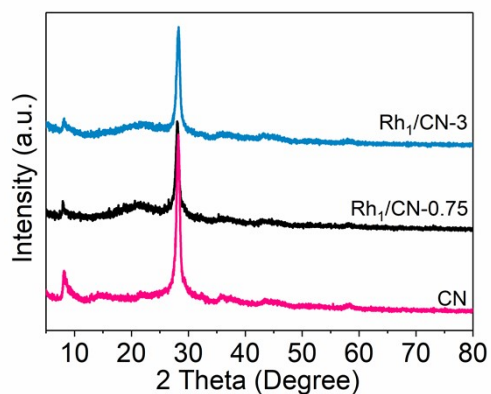


Fig. S1 XRD patterns of CN, Rh₁/CN-0.75, and Rh₁/CN-3.

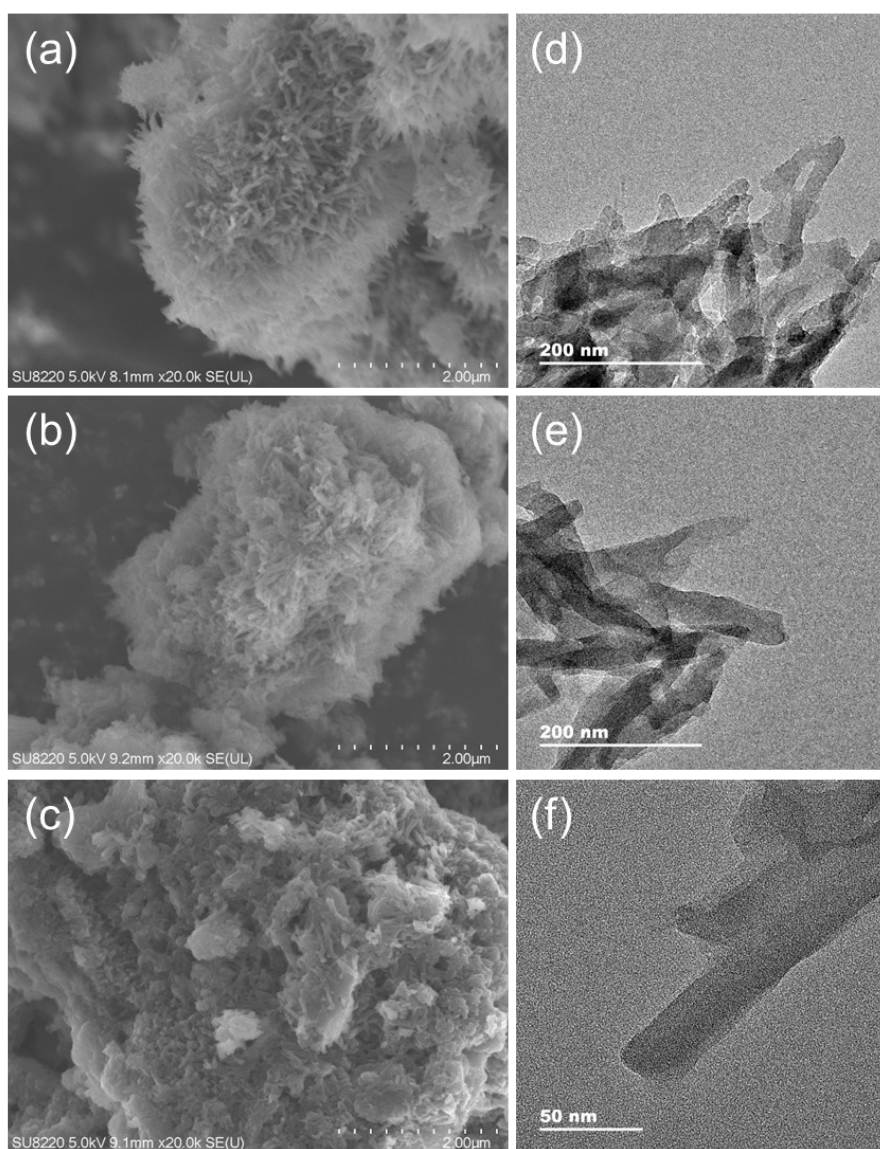


Fig. S2 SEM images of CN (a), Rh₁/CN (b), and Rh₁-bpy/CN (c); TEM images of CN (d), Rh₁/CN (e), and Rh₁-bpy/CN (f).

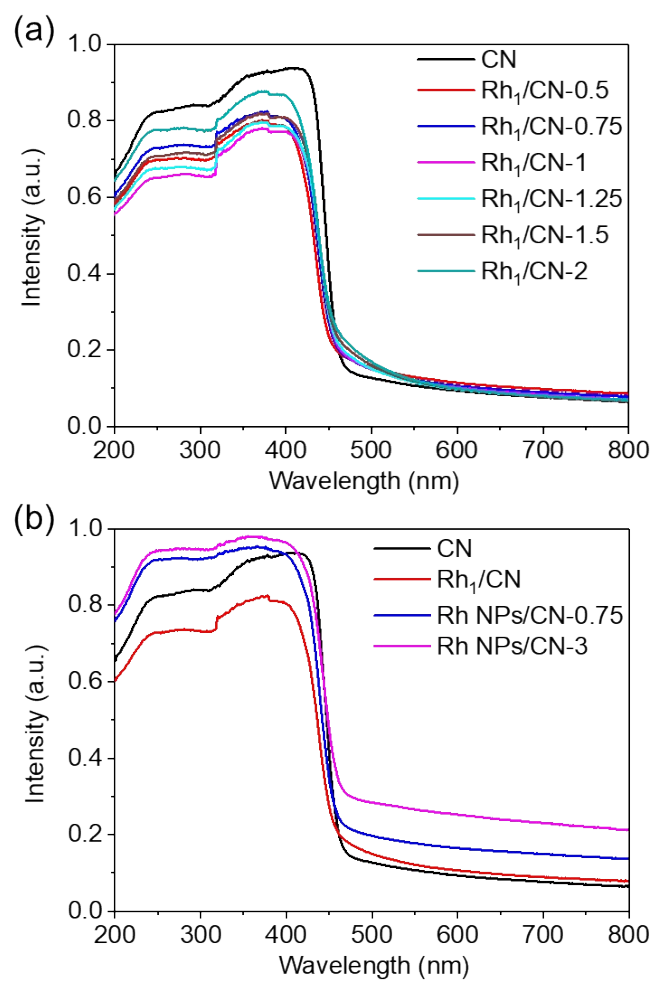


Fig. S3 (a) UV-vis DRS spectra of CN and Rh₁/CN-x with different Rh contents; (b) UV-vis DRS spectra of CN, Rh₁/CN, and Rh NPs/CN -x with different Rh contents.

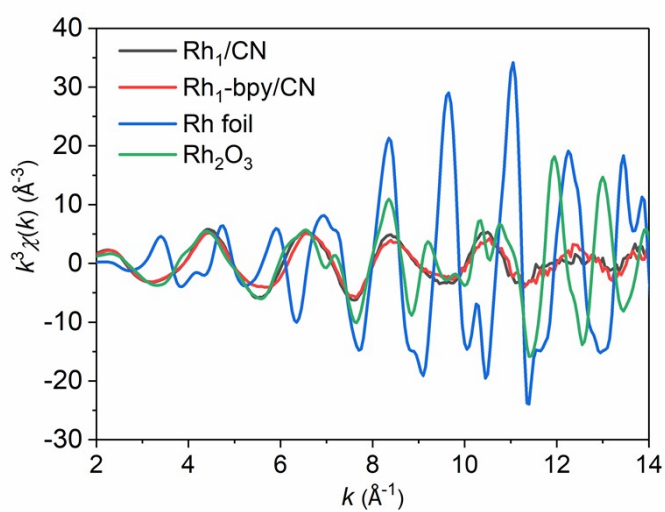


Fig. S4 The experimental k^2 -weighted scattering functions of Rh foil, Rh₂O₃, Rh₁/CN, and Rh₁-bpy/CN.

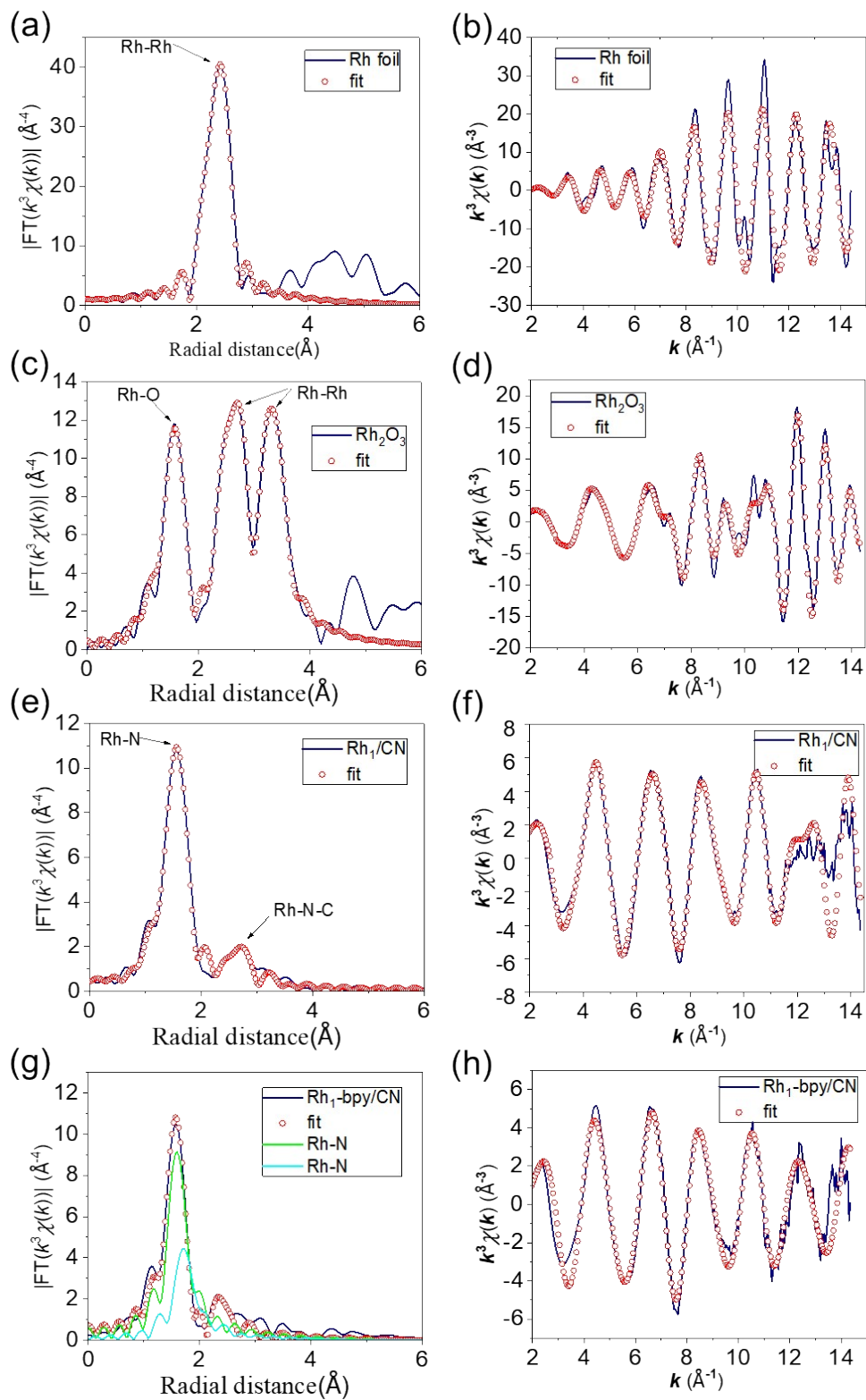


Fig. S5 Experimental and fitted Ti K-edge Fourier transform EXAFS spectra of Rh foil (a and b), Rh_2O_3 (c and d), Rh_1/CN (e and f), and $\text{Rh}_1\text{-bpy}/\text{CN}$ (g and h).

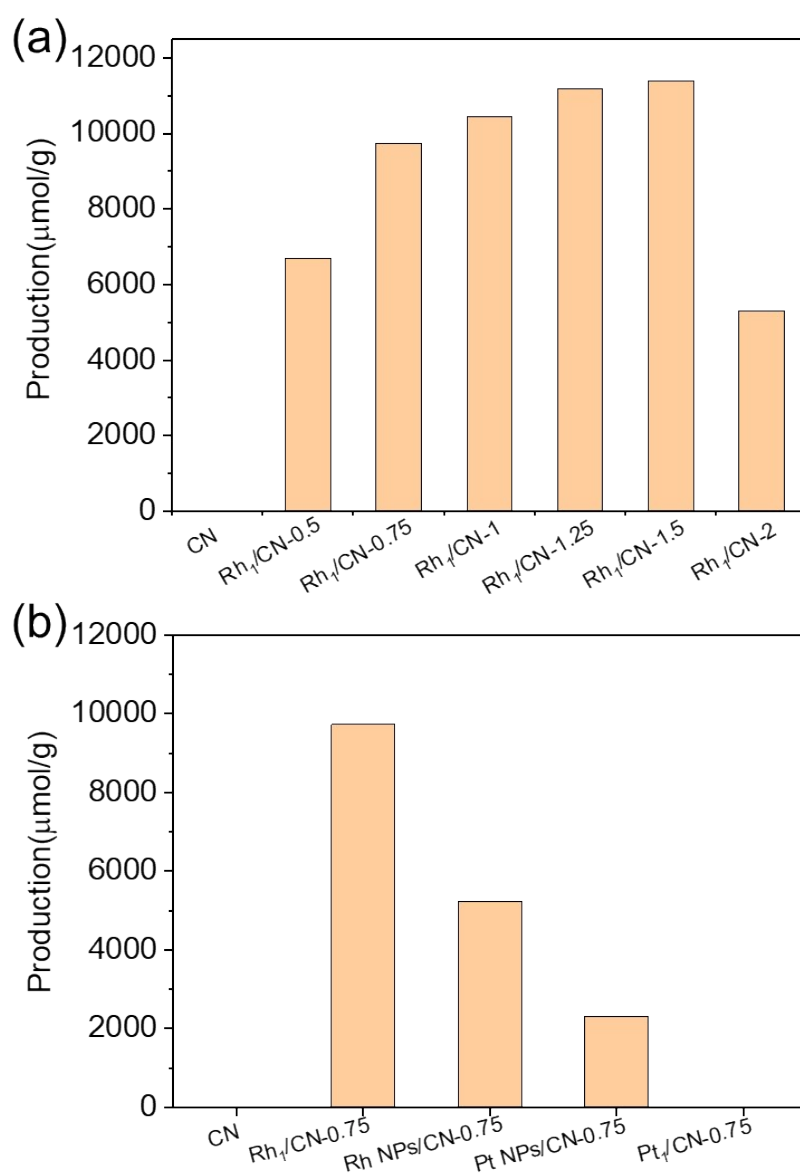


Fig. S6 (a) photocatalytic H₂ evolution over CN and Rh₁/CN-x with different Rh contents; (b) photocatalytic H₂ evolution over CN, Rh₁/CN-0.75, Rh NPs/CN-0.75, Pt NPs/CN-0.75, and Pt₁/CN-0.75.

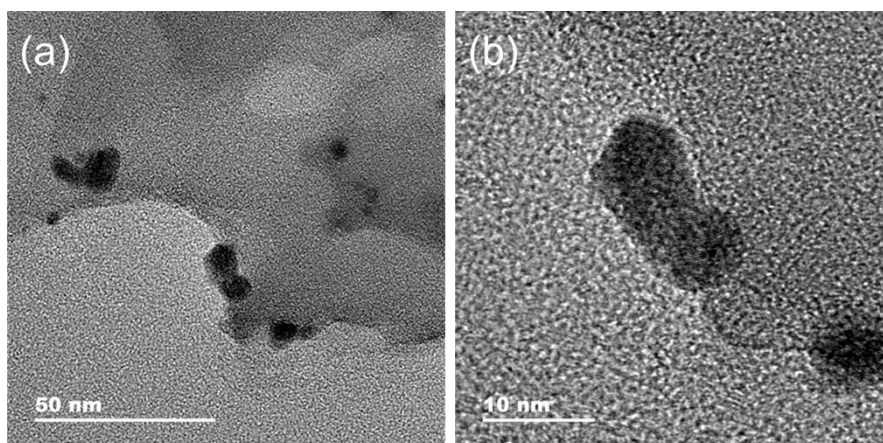


Fig. S7 TEM (a) and HRTEM (b) images of Rh NPs/CN-3.

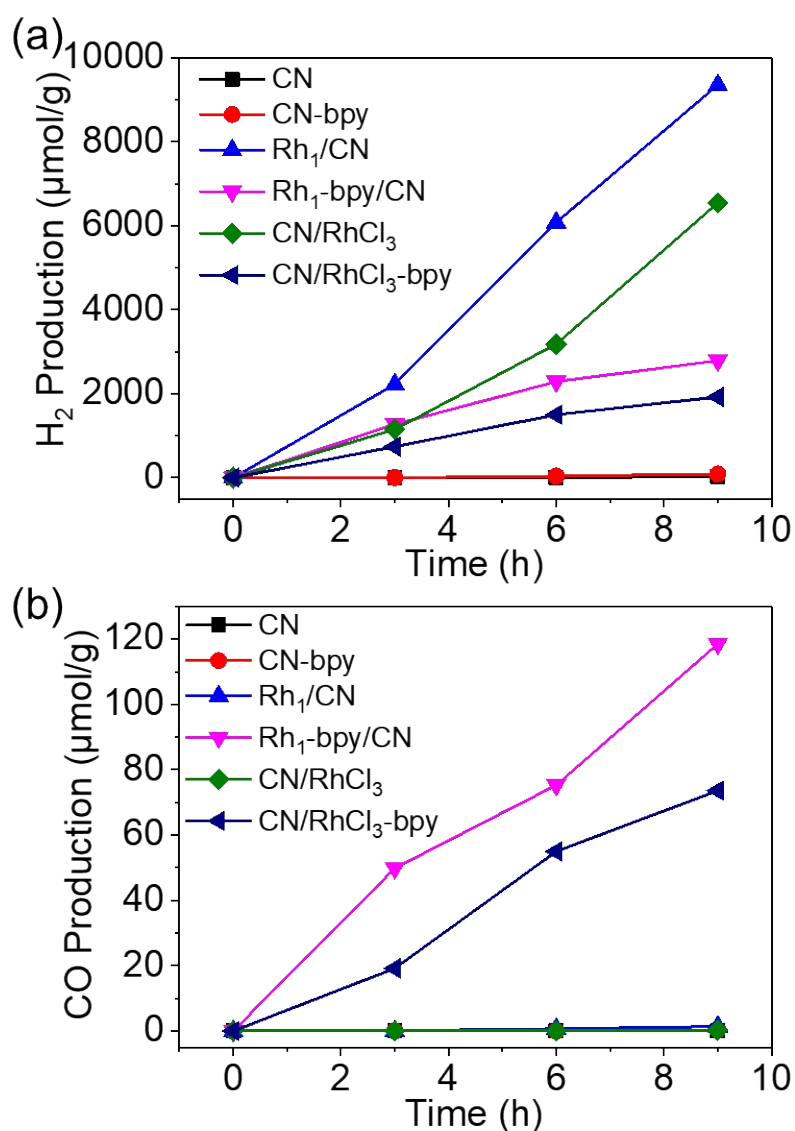


Fig. S8 Time-dependent photocatalytic CO and H₂ evolution over CN, CN-bpy, CN/RhCl₃, CN/RhCl₃-bpy, Rh₁/CN, and Rh₁-bpy/CN under solar light irradiation.

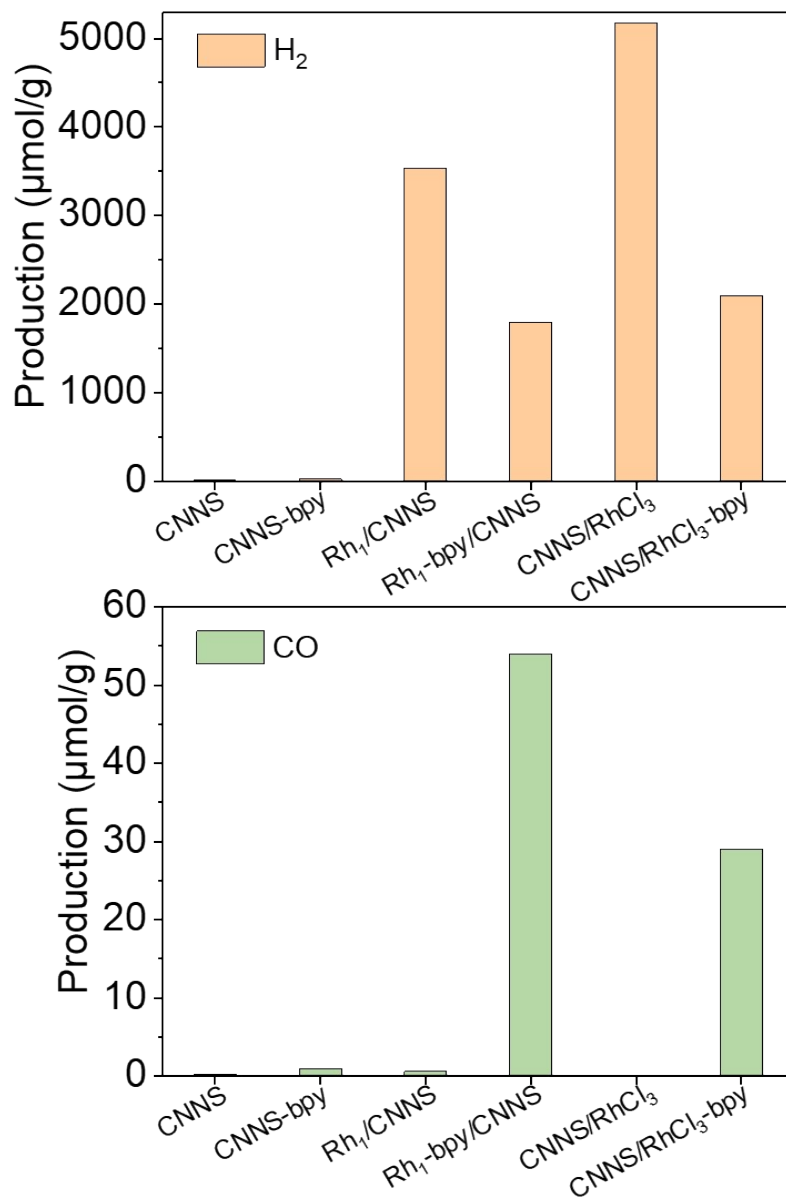


Fig. S9 photocatalytic CO and H₂ evolution over CNNS, CNNS-bpy, CNNS/RhCl₃, CNNS/RhCl₃-bpy, Rh₁/CNNS, and Rh₁-bpy/CNNS under solar light irradiation.

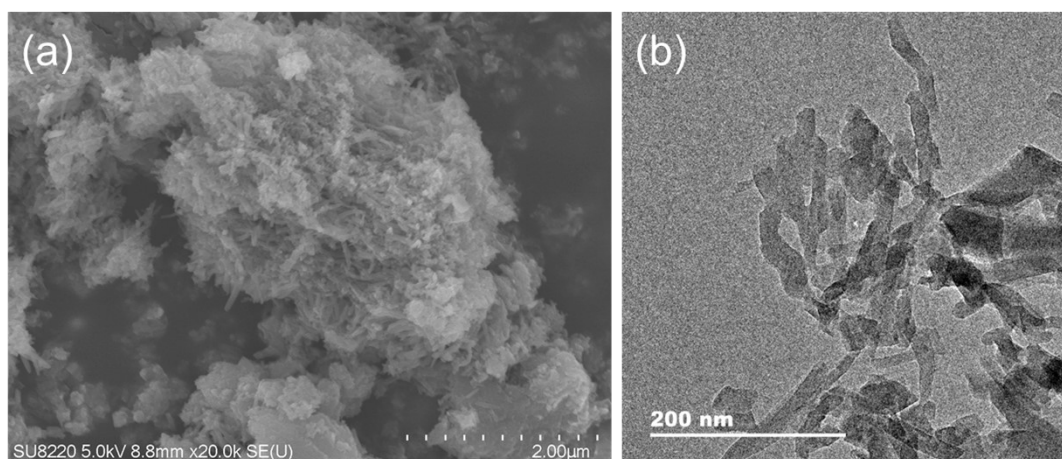


Fig. S10 SEM (a) and TEM (a) images of CN/RhCl₃-bpy.

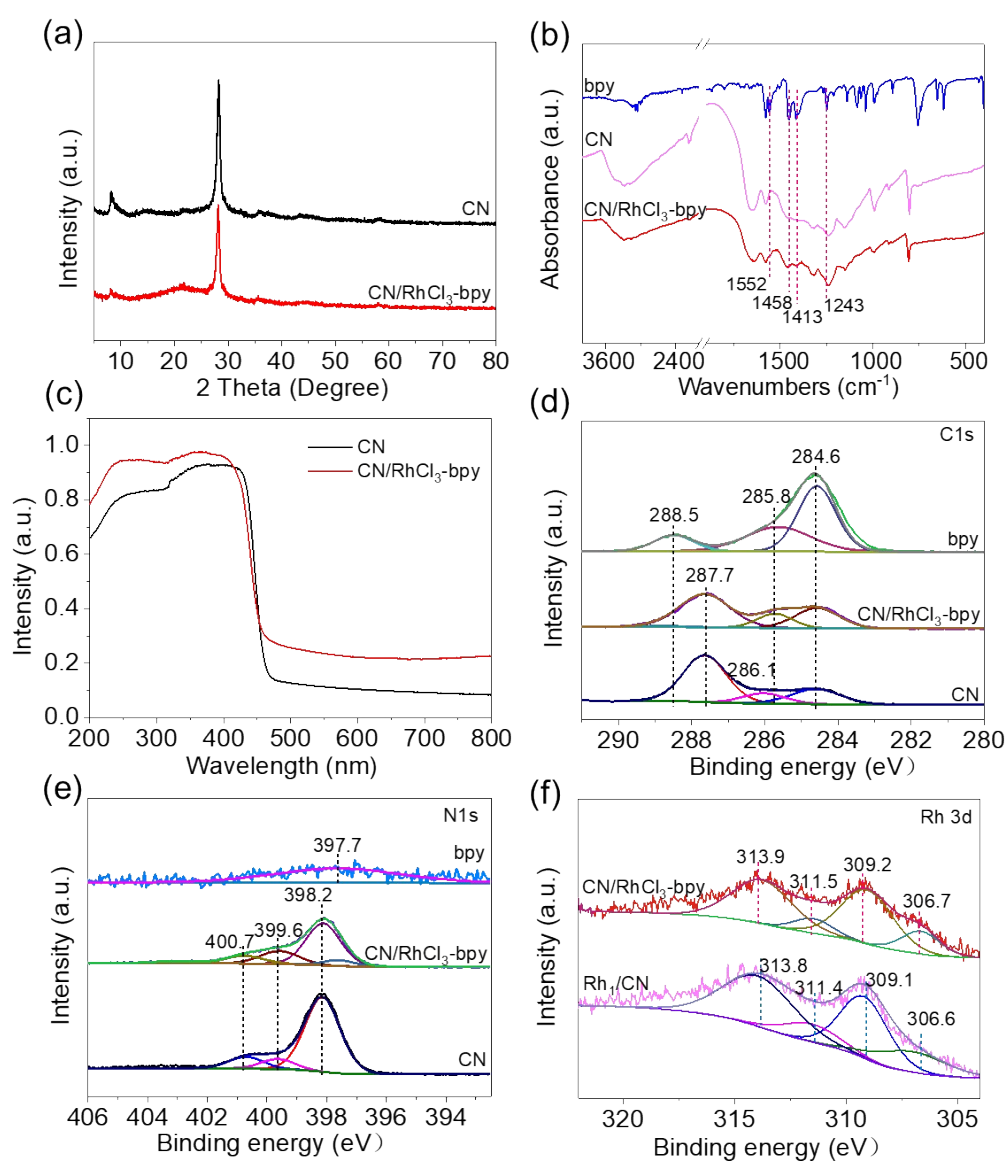


Fig. S11 XRD pattern (a), FTIR spectra (b), UV-vis DRS spectra (c), high-resolution C 1s (d), N 1s (e), and Rh 3d (f) XPS spectra of CN/RhCl₃-bpy.

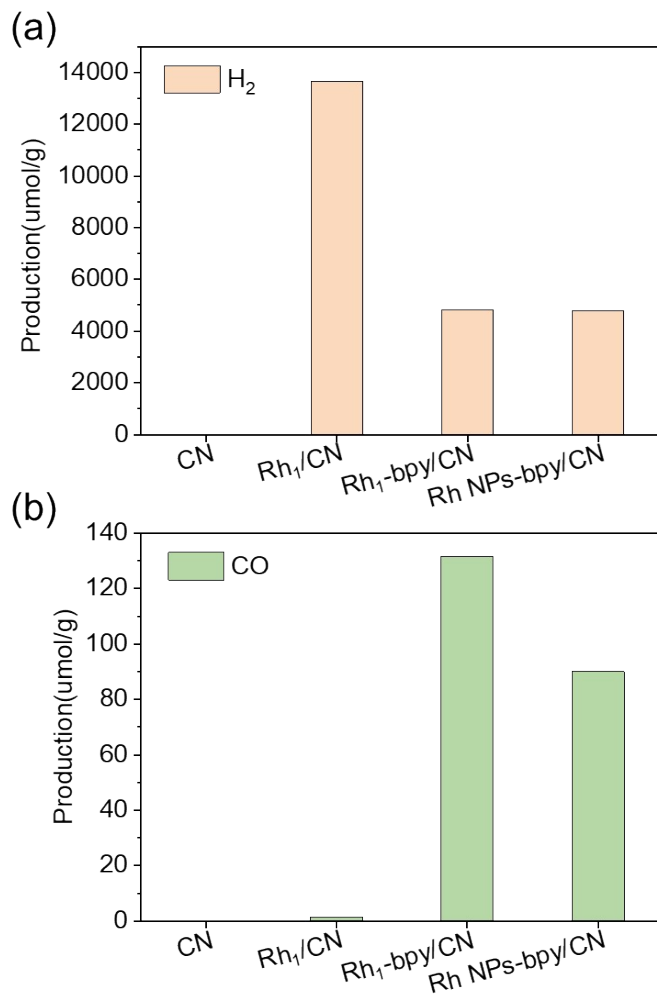


Fig. S12 photocatalytic CO and H₂ evolution over CN, Rh₁/CN, Rh₁-bpy/CN, and Rh NPs-bpy/CN under solar light irradiation.

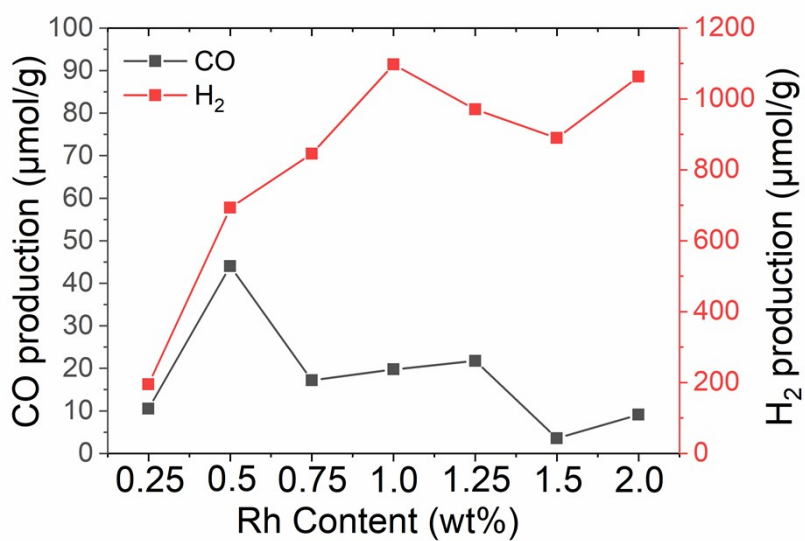


Fig. S13 Effect of Rh contents on the photocatalytic activities of Rh₁/CN-bpy under visible light irradiation.

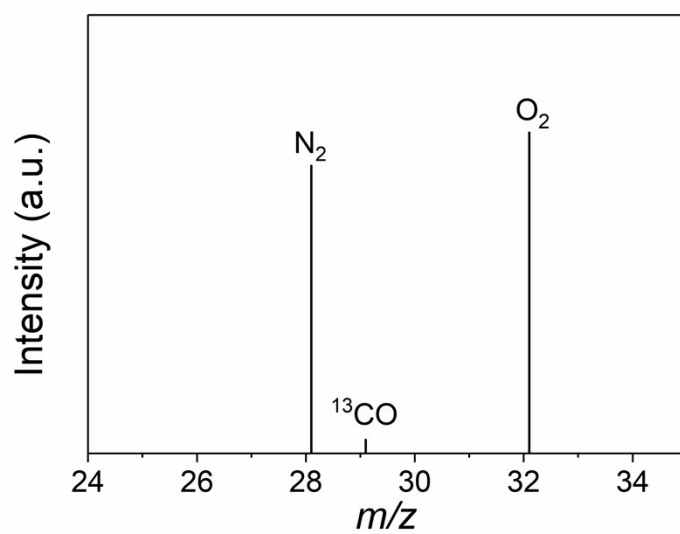


Fig. S14 ¹³C isotope labeling experiment for photocatalytic CO₂ reduction to CO.

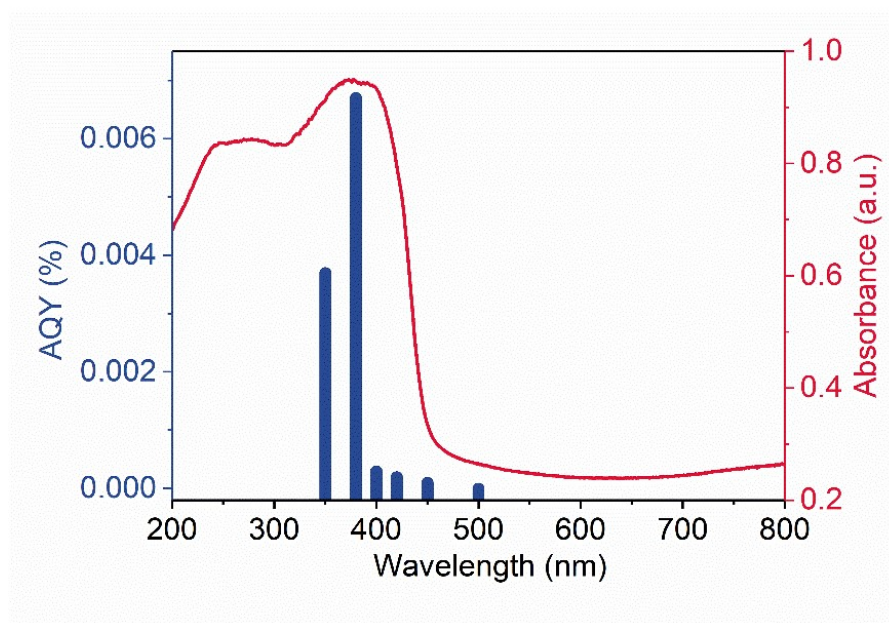


Fig. S15 Wavelength-dependent of the apparent quantum efficiency for CO evolution on Rh₁-bpy/CN.

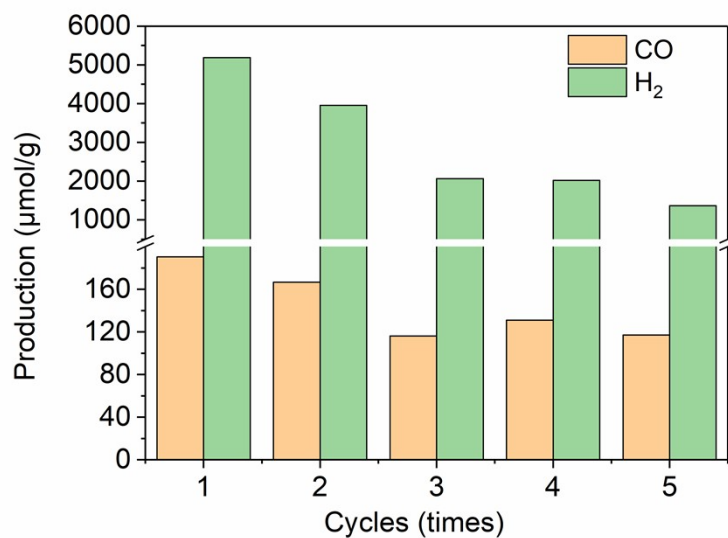


Fig. S16 Photocatalytic CO₂ reduction activity of Rh₁/CN-bpy for successive five cycles under solar light irradiation.

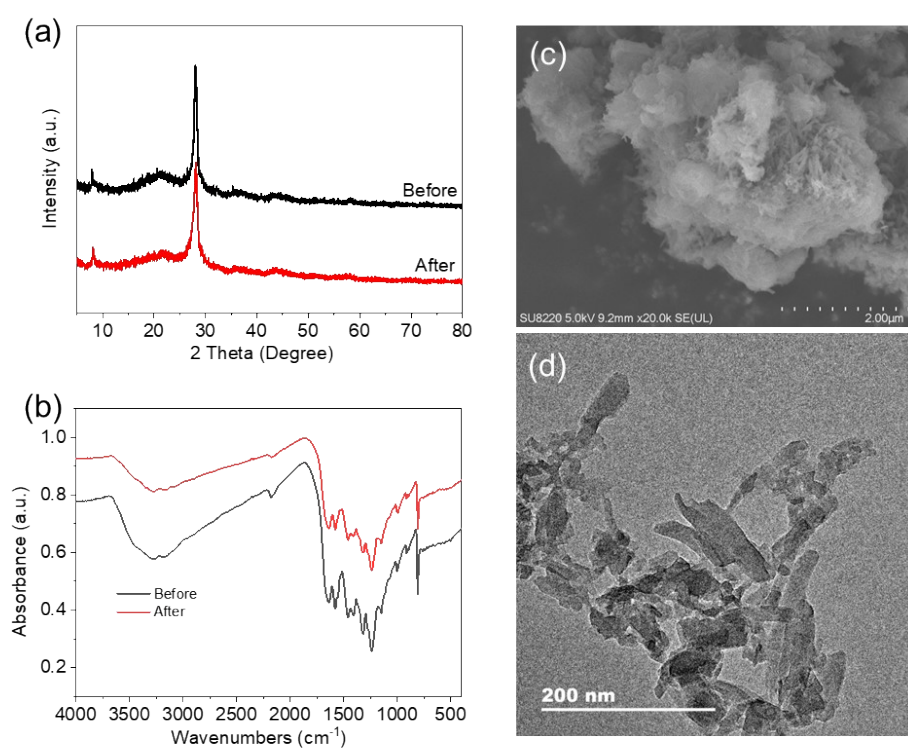


Fig. S17 XRD patterns (a), FTIR spectra (b), SEM image (c), and TEM image (d) of Rh₁/CN-bpy after successive five cycles.

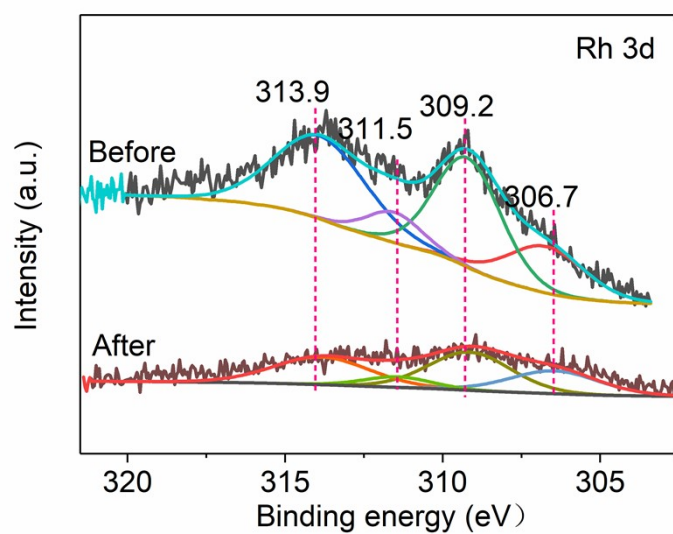


Fig. S18 the high-resolution Rh 3d XPS spectra of Rh₁-bpy/CN photocatalyst before and after the cycling tests.

Table S1 Comparison of CO₂ reduction activity of Rh₁/CN-bpy under different conditions.

Entry	Rh ₁ - bpy/CN	Light	2,2'- bipyridine	TEOA	CH ₃ CN	H ₂ O	CO ₂	CO (μmol/g)	H ₂ (μmol/g)
1	√	√	√	√	√	√	√	131.5	4814.5
2	√	√	√	√	√	√	Ar	0	8641.5
3	√	√	-	√	√	√	√	1.4	13647.5
4	√	√	√	-	√	√	√	0.04	66
5	√	√	√	√	-	√	√	1.9	1199.5
6	√	√	√	√	√	-	√	43.5	4250
7	-	√	√	√	√	√	√	0	0
8	√	-	√	√	√	√	√	0	0